Q. J. R. Meteorol. Soc. (2004), **130**, pp. 2459–2474 doi: 10.1256/qj.04.28

Interannual variability of stratospheric trace gases: The role of extratropical wave driving

By J. MA[1], D. W. WAUGH[2]* A. R. DOUGLASS[3], S. R. KAWA[3], P. A. NEWMAN[3], S. PAWSON[3], R. STOLARSKI[3] and S. J. LIN[4]

[1]*Computational Physics Inc., Springfield, USA*
[2]*Department of Earth and Planetary Sciences, Johns Hopkins University, Baltimore, USA*
[3]*NASA Goddard Space Flight Center, Greenbelt, USA*
[4]*NOAA GFDL, Princeton, USA*

(Received 23 February 2004; revised 19 May 2004)

SUMMARY

The interannual variability of methane and ozone from a 35-year middle atmosphere climate model simulation with no interannual variations in external forcing or chemistry is examined. The internal dynamics in the model produces large tracer interannual variability, particularly in polar regions. During winter and spring the interannual standard deviation in the polar lower-middle stratosphere is about 30% of the climatological mean for methane and 15% for ozone. Global-scale, coherent interannual variations in temperature, residual circulation, and tracers are correlated with variability in the extratropical wave forcing. Statistically significant positive correlations between wave driving and polar tracer tendencies, including column ozone, occur from autumn to spring in both hemispheres. These positive correlations imply that interannual variations in polar tracers are dominated by variations in the horizontal eddy transport and not by variations in residual mean descent rates.

KEYWORDS: Ozone Polar vortex Stratospheric transport

1. INTRODUCTION

In recent years there has been a great deal of interest in temporal changes in the composition of the stratosphere, in particular the abundance of ozone, water vapour and other radiatively and photochemically important gases. A key issue is the possible role of anthropogenic activities in causing any changes. To isolate changes due to anthropogenic activities, it is necessary to determine what changes could be produced by 'natural' internal variability within the stratosphere. Numerous modelling studies have shown that internal dynamics within the stratosphere–troposphere system can produce considerable interannual variability in stratosphere meteorology (e.g. Rind *et al.* 1988; Hamilton 1995; Langematz and Pawson 1997; Pawson *et al.* 2000). However, it is not known what interannual variations in stratospheric tracers can be produced by these internal dynamics.

We examine this issue here by analysing methane (CH_4) and ozone (O_3) fields from a simulation with no interannual variability in the external forcing. The only other study, that we are aware of, to have examined 'natural' tracer interannual variability is Wong *et al.* (1999), who examined the variations in N_2O and CFC-11 budgets and lifetimes from a six-year simulation. They did not, however, examine in detail the variations in the tracer distributions. Also, six years is too short to fully characterize the interannual variability, especially in polar regions.

The simulated CH_4 and O_3 fields examined here are from an off-line three-dimensional chemical transport model (3D CTM) driven by winds from a 35-year integration of a general circulation model (GCM) with no interannual variability in the external forcing (e.g. climatological sea surface temperatures and fixed radiative gases). Furthermore, there are no interannual variations in the parametrized chemistry used in

* Corresponding author: Department of Earth and Planetary Sciences, Johns Hopkins University, 3400 N Charles St, Baltimore, MD 21218, USA. e-mail: waugh@jhu.edu

the CTM. Hence, all interannual variations in the tracers are due to the internal dynamics of the GCM. Using these simulated fields, we examine what interannual variations in stratospheric tracers can be produced by internal dynamics, and how these tracer variations are related to variations in the stratospheric circulation.

The model simulations are described in the next section. In section 3 we briefly describe the climatological structure of the Finite-Volume GCM (FVGCM) simulation, and compare it with meteorological analyses. The climatological structure of the tracers is then presented and compared with observations in section 4. The relationships between the variability in the dynamical and tracer fields is examined in section 5. Concluding remarks are in section 6.

2. Model and simulations

The distributions of methane and ozone examined here are from simulations using a simplified version of the NASA Goddard Space Flight Center (GSFC) off-line 3D CTM (Douglass *et al.* 1997; Douglass and Kawa 1999). Constituents are transported using the advection scheme of Lin and Rood (1996), but parametrized, rather than full, chemistry is used. The parametrized chemistry uses 'look-up' tables of the coefficients of production, and linear and quadratic loss of the tracers that are functions of latitude, height, and month. (For methane only a linear loss term is used.) These coefficients have been archived from an explicit full chemistry solution by the Commonwealth Scientific and Industrial Research Organisation (CSIRO) 2D photochemical transport model (Randeniya *et al.* 1997), and were used in the 3D CTM simulations of Waugh *et al.* (1997). There was no polar heterogeneous chemistry in the 2D model run. Although there are seasonal variations, there are no interannual variations in the chemical production and loss rates. The tracer mixing ratios are fixed at constant values (10 parts per billion (ppb) for O_3 and 1740 ppb for CH_4) in the bottom three levels of the CTM (surface to 650 hPa). The initial tracer distributions were formed by running the CTM for five years using the first year of winds, by when the tracer distributions were annually repeating.

The meteorological fields used in the CTM are from a 35-year integration of the National Aeronautics and Space Administration/National Center for Atmospheric Research (NASA/NCAR) FVGCM. The CTM is run at horizontal resolution 2.5° longitude by 2° latitude with 35 levels from the surface to 0.04 hPa. This has the same horizontal resolution but a slightly lower lid and fewer levels than the FVGCM (which has 55 levels with top at 0.01 hPa). The FVGCM uses a flux-form semi-Lagrangian transport scheme and a quasi-Lagrangian vertical coordinate system to ensure accurate representation of transport by the resolved-scale flow (Lin *et al.* 2004). Physical parametrizations are based on those used in Version 3 of the NCAR Community Climate Model (Kiehl *et al.* 1998), and the gravity wave drag parametrization is similar to that of Boville (1995). The FVGCM simulation used prescribed, annually repeating sea-surface temperatures, sea-ice distributions, radiative gases, and incoming solar radiation. There is no interannual variability in the external forcing, hence all interannual variations in the meteorological fields are internally generated. There is a weak semi-annual oscillation (SAO) but no quasi-biennial oscillation (QBO) in the FVGCM simulation.

3. Meteorology

Before examining the tracer distributions, we very briefly describe the meteorological fields produced by the FVGCM simulation and compare these with the corresponding fields from the US National Centers for Environment Prediction (NCEP) Climate

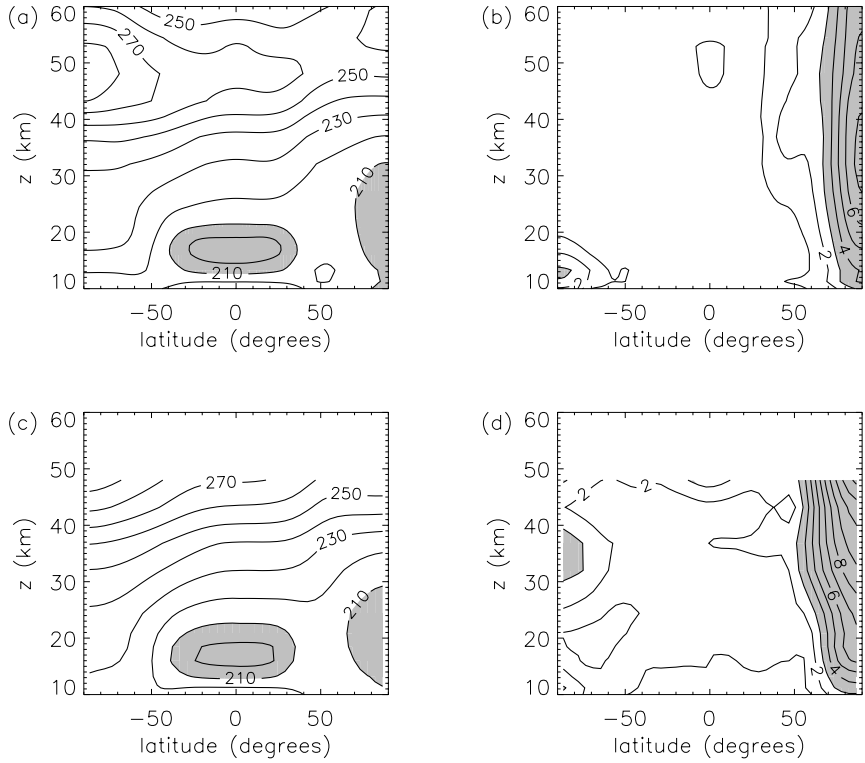

Figure 1. January-mean zonal-mean temperature versus height and latitude from 35-year model simulation: (a) climatological mean with contour interval 10 K and values below 210 K shaded, and (b) interannual standard deviation with contour interval 1 K and values above 3 K shaded. (c) and (d) are as (a) and (b) respectively, but from 24 years of CPC analyses.

Prediction Center (CPC) stratospheric analyses (Gelman *et al.* 1986; Randel 1992), for the period October 1978 to June 2002.

The 35-year FVGCM simulation used in the CTM reproduces the main climatological features of the stratospheric meteorology, and overall there is very good agreement with the climatology from CPC (and other) analyses. As an example, Figs. 1(a) and (c) show the climatological January-mean zonal-mean temperature from the FVGCM simulation and CPC analyses. The minimum temperature in the northern (winter) polar region is within 0.5 K of the observed value, and the tropical tropopause temperature is within 3 K of that observed. Other important climatological features are also captured, including the annual cycle and minimum values of temperatures at the tropical tropopause and at both poles.

As found in other studies (e.g. Rind *et al.* 1988; Boville 1995; Hamilton 1995; Langematz and Pawson 1997), even though there is no interannual variability in the external forcing of the FVGCM there is considerable interannual variability in the stratospheric meteorology (especially at high latitudes during winter and spring). Furthermore, this variability is comparable with that in the meteorological analyses. This is illustrated in Figs. 1(b) and (d) which show the interannual standard deviation of January temperature for the model and the CPC analyses. The standard deviations in the model are slightly smaller than in the analyses. This is the case for January to March,

whereas in early winter the opposite is true. This seasonal difference between model and observed variability has been found in other GCMs (e.g. Hamilton 1995).

The model also reproduces the main features of the observed temperature variability in the southern polar region. The temperature variability in early and midwinter is similar to that observed, although the model standard deviation is slightly larger than observed in late winter (e.g. September) and slightly smaller in spring (November–December). There are also some differences in altitude of the peak variability, but these differences are generally small, and overall there is good agreement.

There is also interannual variability in the tropical upper stratosphere of the model, but it is weaker than observed, e.g. the standard deviations in the model temperature are around 1 K compared with values around 3 K from the CPC analyses (see Fig. 1). The model–data differences in the variability of the tropical winds are even larger; the observed interannual standard deviations increase from around 4 m s^{-1} at 20 km to over 8 m s^{-1} at around 40 km, whereas in the model the values are around or less than 2 m s^{-1}. These differences are because the model produces only a weak SAO and no QBO, and have been found in other studies (e.g. Boville 1995).

4. Trace gases

The above comparisons show that the simulated meteorology is fairly realistic, both in terms of the climatological structure and interannual variability. The one exception is within the tropics, where the model lacks a QBO and has weaker interannual variability. We now examine the climatological structure and interannual variability of the methane and ozone fields produced by the model, and compare with observations. Given the deficiencies in the tropical meteorology we focus on the tracer variability in the extratropics.

(*a*) *Climatological fields*

The climatological January zonal-mean CH_4 and O_3 fields from the model are shown in Fig. 2. Also shown are climatological January-mean CH_4 and O_3 fields from the Upper Atmosphere Research Satellite (UARS) reference climatology*. There is reasonable agreement between the model and observations for both tracers.

The shape of the CH_4 isopleths is similar in the model and observations, with both having steep meridional gradients at the edges of the tropics and at the edge of the winter polar vortex. There is also good agreement in the seasonal shift in the location of high tropical values (not shown). There are, however, some discrepancies. In particular, there is no double-peak structure in the simulated tropical upper-stratospheric CH_4, a consequence of the weak SAO in the FVGCM.

The simulated O_3 climatology also reproduces the main features of the observations: the maximum volume mixing ratio occurs in the tropical middle stratosphere, there are strong vertical gradients in the lower stratosphere, and strong meridional gradients in the middle stratosphere in middle to high latitudes. However, the modelled tropical mixing ratio peak is larger than in the UARS climatology, and, as in many other simulations (e.g. Prather and Remsberg 1993; Park *et al.* 1999), the modelled peak in midlatitudes is 2 to 5 km too low.

The main spatial and temporal variations in total-column ozone are also reproduced by the model. Figures 3(a) and (c) show the climatological zonal-mean column-integrated O_3 from the model and from the Total Ozone Mapping Spectrometer (TOMS)

* http://code916.gsfc.nasa.gov/Public/Analysis/UARS/urap/home.html

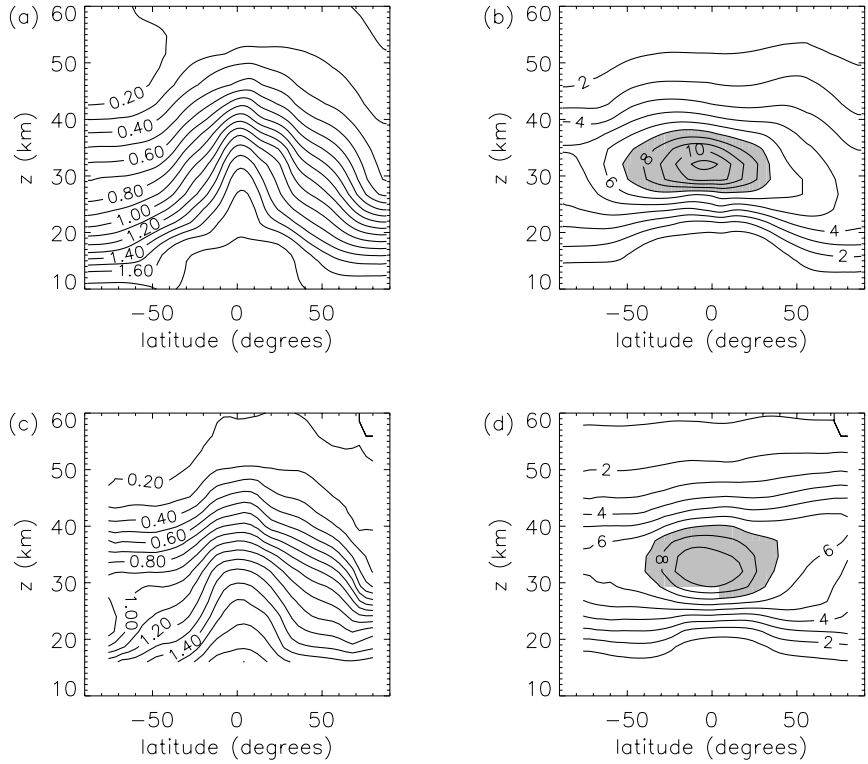

Figure 2. Model climatological January-mean values of zonal-mean (a) CH_4 with contour interval 0.1 ppmv, and (b) O_3 with contour interval 1 ppmv, with values greater than 7 ppmv shaded. (c) and (d) are as (a) and (b), but show UARS reference climatology.

and Solar Backscatter Ultraviolet (SBUV and SBUV/2) merged dataset*. The location and timing of the high-latitude peak values and seasonal evolution of the tropical minimum agree well with observations. However, the peak values in polar regions during spring are larger than observed (especially in the northern hemisphere) while the tropical values are too low by around the same amount.

(*b*) *Interannual variability*

As with the meteorological fields, there is considerable interannual variability in CH_4 and O_3. The variability in the two tracers occurs in roughly the same regions and seasons, with both having largest standard deviations in the polar middle stratosphere (e.g. Fig. 4). For both tracers the standard deviations in polar regions are sizeable fractions of the climatological mean values, e.g. the standard deviations at the North Pole and 30 km in January are around 30% of the climatological mean for CH_4 and around 15% for O_3. In the northern polar regions there are large interannual standard deviations for both tracers (above 0.05 ppmv for CH_4 and above 0.4 ppmv O_3) from autumn to early summer, whereas the standard deviations in southern polar regions are small during midwinter and large values occur only from late winter to summer (e.g. Figs. 4(c) and (d)). Another hemispheric difference is that the maximum variability is always in polar regions in the northern hemisphere, whereas during southern winter

* http://code916.gsfc.nasa.gov/Data_services/merged/mod_data.public.html

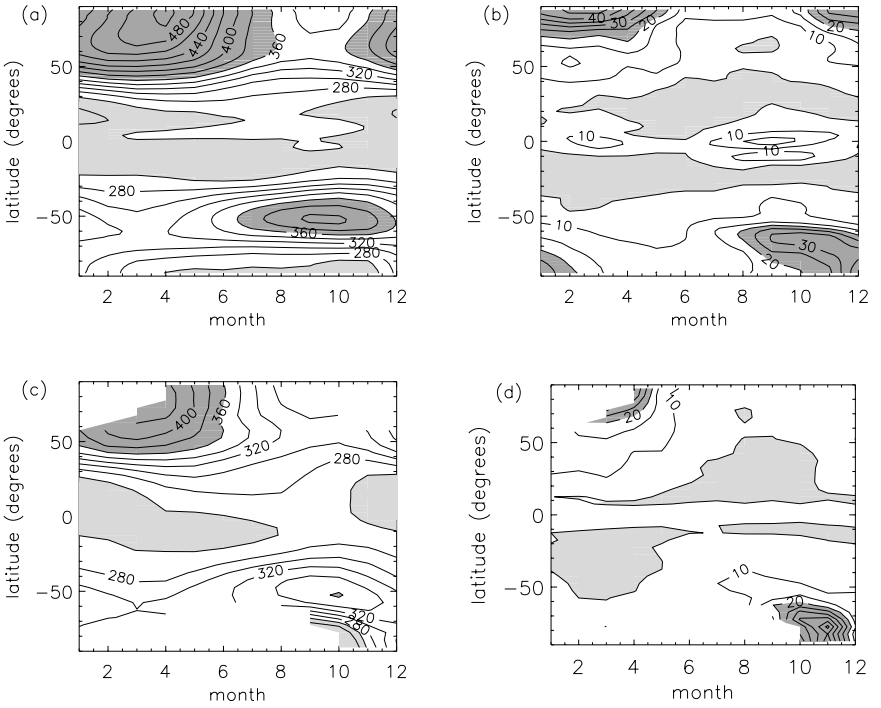

Figure 3. Annual variation versus latitude of zonal-mean values of total-column ozone from the model: (a) climatological mean with contour interval 10 DU, light shading below 270 DU and dark shading above 360 DU, and (b) interannual standard deviation with contour interval 5 DU, with light shading below 5 DU and dark shading above 20 DU. (c) and (d) are as (a) and (b), but from TOMS-SBUV.

(June–August) it is located off the pole. In both hemispheres the altitude of maximum variability descends with time. For example, in the northern hemisphere the maximum standard deviations are centred around 30–35 km in November, but descend through winter and in April and May are centred around 25 km.

The regions of large interannual variability of tracers are in roughly the same regions as those of temperature, e.g. compare Figs. 4 and 1. However, whereas the temperature variability in polar regions is large throughout the depth of the stratosphere, the largest tracer variability occurs in a more limited altitude range, where the tracer gradients are large (e.g. between 20 and 40 km in northern polar regions in January). Also, polar tracer variability persists longer into the summer than that of temperature, e.g. the interannual standard deviation of lower stratospheric ($\approx$25 km) ozone in the northern polar region remains above 0.3 ppmv throughout the year (Fig. 4).

There are also large interannual standard deviations in the column-integrated O_3: Figs. 3(b) and (d) show the standard deviations for total-column O_3 from the model and TOMS-SBUV data. (As the model does not produce an ozone hole, a linear trend has been removed from the TOMS-SBUV data before calculation of the standard deviation. This, however, makes only a small difference.) Because lower stratospheric ozone dominates the column and there is virtually no interannual variability in upper stratospheric O_3 in the model, the latitudinal and temporal variations of the model column O_3 are very similar to those of the O_3 mixing ratio in the lower stratosphere (Fig. 4(d)). There is reasonable agreement between model and data, with both showing largest variability in polar regions (with maximum values in spring) and minimum

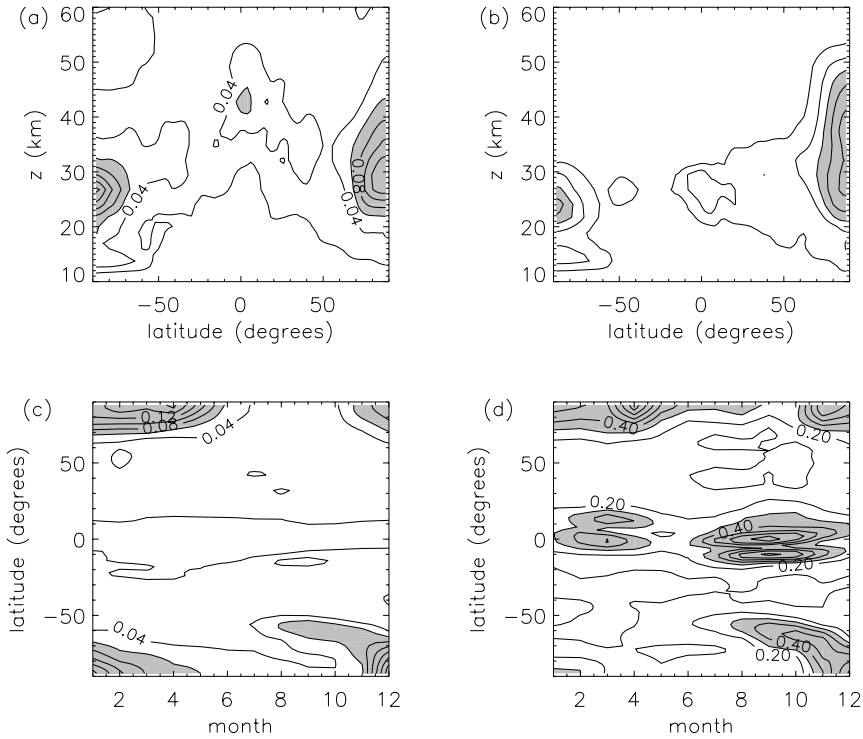

Figure 4. Interannual standard deviation of model zonal means: January height–latitude section for (a) CH_4 and (b) O_3, and latitude–month section at 27 km for (c) CH_4 and (d) O_3. Contour interval in (a) and (c) is 0.02 ppmv, with values above 0.06 ppmv shaded, while contour interval in (b) and (d) is 0.1 ppmv, with values above 0.3 ppmv shaded.

values in the subtropics. The magnitude of the variability in northern spring is very similar in model and data, but the model underestimates the magnitude in southern spring. In both the model and data, the standard deviation in the tropics is around 5–10 DU (although the model shows a large seasonal cycle which is absent in the data).

Further aspects of the temporal variability of the simulated total column O_3 can be seen in Fig. 5, which shows the latitudinal and temporal variations of deseasonalized anomalies of total O_3. The anomalies shown are formed by removing the climatological monthly mean values from each monthly value, and then smoothing using a 24-month running time mean. As expected from the above plots of the interannual standard deviations, the anomalies are largest in polar regions and smallest in the subtropics, and there is reasonable agreement with observations (e.g. Figure 1 of Randel and Wu (1996)). This figure shows that the interannual variability in total O_3 includes anomalies that can persist for many years. In particular, 10- to 15-year periods can be found when there are large increasing or decreasing 'trends'. For example, there is a decreasing trend in total O_3 in southern polar regions during the mid 1950s to late 1960s, which is followed by a large upward trend over the next 10 years. Even larger trends can be found in the model if only springtime O_3 is considered, e.g. linear trends in October-mean 60–90°S column ozone are around -25 DU decade^{-1} and $+40$ DU decade^{-1} for 15-year periods beginning at model years 53 and 64, respectively. Large trends also occur for column ozone in northern polar regions, e.g. trends of around -15 DU decade^{-1} occur for March-mean 60–90°N column ozone between model years 50 and 64 and

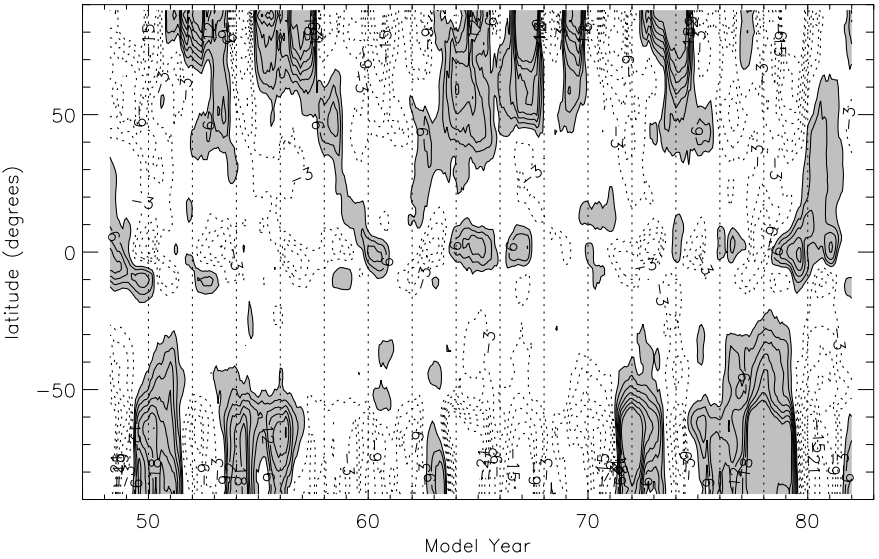

Figure 5. Latitude–time variation of deseasonalized total-column O_3 anomalies (see text for details). Contour interval is 3 DU with dashed contours for negative values, values greater than 3 DU shaded and the zero contour omitted.

between years 66 and 81. Smaller trends can also be found in midlatitude ozone, e.g. northern midlatitude (20–60°N) deseasonalized ozone has a negative trend of around 7 DU decade^{-1} for 15 years between model years 64 and 79. We are currently analysing the characteristics of these multiyear variations in more detail.

5. Relationships between dynamics and tracers

The above analysis has shown that, even with no interannual variations in the external forcing or chemistry, the model produces large interannual variability in both meteorology and tracers. We now examine the relationships between the different fields. We use cross-correlations to examine the spatial structure, in the meridional plane, of interannual variations in the different fields. At each latitude and height the 35-year time series of monthly mean values of a given field are correlated with the reference 35-year time series of a specified field at the given location. For 35-year time series, correlations of 0.33 and 0.43 are significant at the 95% and 99% confidence levels.

We focus first on the northern hemisphere relationships in January, and then discuss other months and the southern hemisphere.

(*a*) *Meteorology*

We first examine how the variability in stratospheric meteorological fields is related to that of the planetary wave activity entering the stratosphere. Figure 6 shows meridional cross-sections of the interannual correlations of January-mean zonal-mean temperature, $\overline{T}$, and vertical components of the residual circulation, $\overline{w^*}$, with the time series of meridional eddy heat flux, $\overline{v'T'}$, in northern middle latitudes at 100 hPa. The eddy heat flux is proportional to the vertical component of the Eliassen–Palm (E–P) flux, and is a measure of the wave driving of the stratosphere (Andrews *et al.* 1987). For the $\overline{w^*}$ correlations, the heat flux values are for the same month (January), but for the $\overline{T}$ correlations it is more appropriate to consider a time-integrated eddy heat

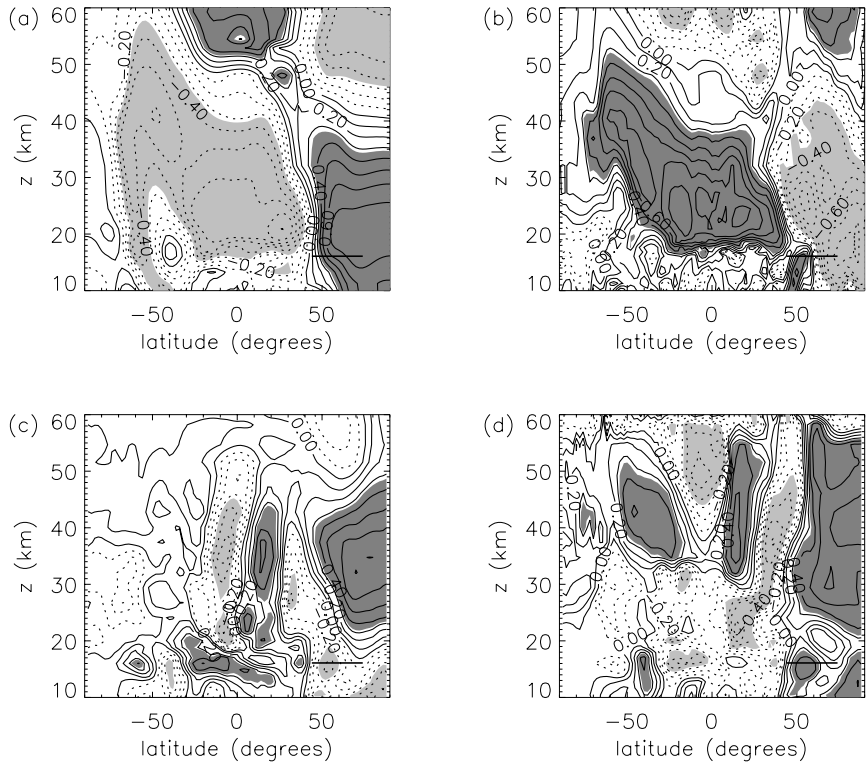

Figure 6. Interannual correlations of January (a) T, (b) $\overline{w^*}$, (c) CH_4 and (d) O_3 with 100 hPa eddy heat flux $\overline{v'T'}$ averaged between 45 and 75°N. For $\overline{w^*}$ the correlations are calculated with the January heat flux, whereas for the other fields the correlation is with the December–January mean heat flux. Contour interval is 0.1, with dashed contours for negative values. Shaded regions are significant at the 95% confidence level (dark shading for positive correlations and light for negative correlations).

flux (see Newman *et al.* 2001), so we use the December–January mean heat flux as the reference time series.

Figure 6(a) shows that $\overline{T}$ is highly correlated with the 100 hPa $\overline{v'T'}$ for most of the stratosphere (the correlations in the shaded regions are significant at the 95% confidence level). The temperature response is out of phase between high and low latitudes, and also between the lower-middle stratosphere and the mesosphere. Temperatures are higher in the polar lower stratosphere and lower within the tropical lower stratosphere in years with increased wave driving, and the reverse occurs in the mesosphere. There is also a strong correlation between the high-latitude zonal winds and the 100 hPa eddy heat fluxes, with weaker winds when there are increased heat fluxes (not shown). This is consistent with thermal wind balance, as there are weaker zonal winds when there are higher polar temperatures.

The correlations of $\overline{w^*}$ with $\overline{v'T'}$ are very similar to those of $\overline{T}$, with the same global-scale quadrupole pattern although of the opposite sign, see Fig. 6(b). In years with larger wave driving there is, generally, increased tropical ascent and polar descent below 45 km, and decreased tropical ascent and polar descent above this altitude. (Note, as $\overline{w^*}$ is negative in polar regions a negative correlation corresponds to increased descent with higher heat fluxes.) The variability in the horizontal components of the residual circulation, $\overline{v^*}$, is also highly correlated with the wave driving, with increased poleward advection when there are increased heat fluxes (not shown).

The above correlated variability in polar and tropical temperatures, middle latitude winds, and residual circulation is consistent with the expected response due to changes in the wave driving, see the schematic diagram in Fig. 8 of Randel (1993). Also, the strong connection between interannual variations in temperature and eddy heat flux has previously been noted in meteorological analyses (e.g. Waugh *et al.* 1999; Newman *et al.* 2001), as well as in other general-circulation models (e.g. Pawson *et al.* 1995; Austin *et al.* 2003).

(*b*) *Trace gases*

The above analysis suggests that the interannual variations in the thermal structure and residual circulation of the stratosphere are primarily driven by interannual variations in the wave driving. Such changes in the residual circulation should lead to interannual variability in the transport of tracers. This link is examined below.

Figures 6(c) and (d) show the correlation of January-mean mixing ratios of CH_4 and O_3 with the December–January 100 hPa eddy heat fluxes. Very similar correlations are obtained if the change in tracer mixing ratio (tracer tendency) over January is correlated with the January-mean eddy heat flux (see section 5(d) below). As expected, there are significant correlations between the extratropical wave driving and tracers. These correlations are largest in polar regions, with peak correlations at roughly the same altitude as peak interannual standard deviations (e.g. compare with Fig. 4). Between 25 and 45 km there are significant positive correlations for both tracers, and hence increased tracer values when the wave driving is increased. Below this altitude the correlations differ between tracers, with a positive correlation for O_3 and a negative correlation for CH_4.

Comparison of Figs. 6(c) and (d) with Fig. 6(a) implies that there should be a positive correlation between temperature and tracers in the polar lower-middle stratosphere (25–45 km). Direct correlation between these quantities confirms this, and shows that the correlations of CH_4 and O_3 with polar lower stratospheric temperatures are very similar to the correlations with wave driving. The magnitude of the change in tracer values associated with given change in temperature can be determined from the slope of the linear regression between tracers and temperature. Such calculations for mean January fields at the North Pole and 30 hPa yield slopes of around 0.012 ppmv K^{-1} for CH_4 and 0.05 ppmv K^{-1} for O_3. Hence the expected change in lower stratospheric tracers for a 20 K change in the polar temperature is 0.24 ppmv (or 24%) in CH_4 and 1 ppmv (24%) in O_3. Similar differences in polar ozone are observed between the 1998/99 and 1999/2000 winters (Strahan 2002); the January 1999 mean lower stratosphere polar temperatures were higher by around 20 K than in 2000 and polar ozone mixing ratios were higher by around 1 ppmv.

(*c*) *Relative roles of vertical and horizontal transport*

The analysis above shows that in January there are positive tendencies in north polar (60–90°N) CH_4 in the middle stratosphere (25–45 km) when there is increased wave driving (Fig. 6). Given that CH_4 decreases with height (Fig. 2), this positive correlation is inconsistent with enhanced descent forced by increased wave driving; stronger 'unmixed descent' should bring down lower tracer concentrations. In fact, the correlation between $\overline{w^*}$ and CH_4 tendencies is weak and negative (e.g. a value of -0.45 for January 30 hPa), indicating a tendency for larger values with more descent.

These negative correlations between $\overline{w^*}$ and CH_4 could be explained if there is increased poleward transport in years with increased polar descent. CH_4 decreases from

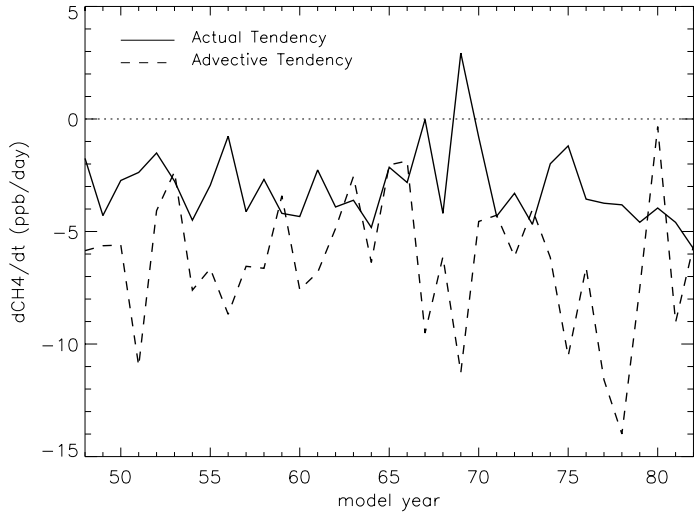

Figure 7. Average tendency in polar average (60–90°) CH_4 at 30 hPa between 28 October and 28 January, for each model year. Solid curve shows actual tendency whereas dashed curve shows tendency due only to advection by the residual mean circulation.

the tropics to the poles, so poleward transport increases tracer values at high latitudes and opposes the effect of descent. Increased poleward advection is in fact consistent with increased residual horizontal velocity, $\overline{v}^*$, when there is increased wave driving. However, this horizontal advection plays only a minor role in the tracer budget (e.g. Randel *et al.* 1994), and there is still a weak negative correlation between the total change in CH_4 and the change due to the combined horizontal and vertical advection (see Fig. 7). The other possible explanation is horizontal eddy transport.

Previous studies have shown that at high latitudes CH_4 and N_2O tendencies are due to small differences between vertical advection and horizontal eddy transport (e.g. Randel *et al.* 1994; Strahan *et al.* 1996). The mean advection term is generally larger, and so over the course of a winter CH_4 decreases. However, even though vertical advection is larger, it is still possible that interannual variability in the tracer is dominated by variability in the horizontal transport. We expect increased wave driving to lead not only to enhanced descent in polar regions but also to more horizontal eddy transport. The above analysis suggests that the interannual variability in this horizontal eddy transport is larger than that in the descent, and dominates the interannual variability in the tracer tendencies.

To examine this further we compare the actual tendency in CH_4 ($\partial\overline{\chi}/\partial t$, where $\overline{\chi}$ is the zonal-mean CH_4 mixing ratio) with that due to advection by the residual mean circulation ($-\overline{v}^*\partial\overline{\chi}/\partial y - \overline{w}^*\partial\overline{\chi}/\partial z$). Figure 7 shows the actual tendency in polar (60–90°N) CH_4 between late October and late January for each winter, together with the time-averaged tendency due to advection. As the chemical sink is negligible in the region considered, the difference between the actual and advective tendency can be used to diagnose the tendency due to eddy transport. (The output from the CTM has been archived only once per week, together with monthly means, which prevents reliable direct calculations of the time-averaged eddy transport.) For all but one year the actual tendency is the same sign as the tendency due to mean advection, however in most years the magnitude of advective tendency is much larger than the actual tendency. This is consistent with the analysis of Randel *et al.* (1994) and Strahan *et al.* (1994). Figure 7 also shows that, even though the actual tendency is usually the same sign as that due to

advection, the interannual variations in the actual tendency do not follow those in the advective tendency. Interpreting the difference between the two curves as the tendency due to eddy transport supports the hypothesis that the interannual variations in the actual tendency are correlated with the variations in the eddy transport.

The correlation between January CH_4 and eddy heat fluxes changes sign around 20 km (see Fig. 6(c); the exact altitude varies with season and between hemispheres). This change in the sign of the correlation could be because poleward transport has only a weak effect on polar CH_4 in the lower stratosphere, and tendencies are dominated by descent. The relative importance of horizontal and vertical transport for tracer dependencies depends on the tracers' horizontal and vertical gradients, and below 20 km there are very weak horizontal CH_4 gradients (Fig. 2), so even large variability in the horizontal transport will have only a small impact on polar CH_4.

The correlations between O_3 and eddy heat fluxes are consistent with the above conclusions. For January, there is a positive correlation between eddy heat fluxes and north polar (60–90°N) O_3 between 25 and 45 km, consistent with dominant role of interannual variations in horizontal transport. (As with CH_4, poleward transport brings in high values of O_3 and descent brings lower values). Below around 25 km, increased descent and increased poleward transport both lead to increased O_3, and correlation between the heat flux and O_3 is still positive below 20 km.

The above analysis has focused on zonal-mean quantities, however an analysis of vortex-averaged CH_4 and diabatic heating rates produces similar results (not shown), with weak negative interannual correlations between CH_4 tendencies and mean heating rates. This indicates that even in a vortex coordinate system the interannual variations in tracers are not correlated with interannual variations in descent.

(*d*) *Other seasons and southern hemisphere*

The analysis in subsections 5(b) and (c) has focused on January-mean quantities. However, significant correlations between wave driving and polar tracers (and temperatures) are also found for other months and in the southern hemisphere. Figure 8 shows the seasonal variation of the correlation between the 100 hPa eddy heat fluxes and the monthly tendency in polar average (60–90°) CH_4 and O_3 at 29 and 22 km, for both hemispheres. (When calculating the southern hemisphere correlation, the negative of the eddy heat fluxes is used, so that positive correlations correspond to increased tracer tendency with increased wave driving.)

There are significant positive correlations between eddy heat fluxes and tracer tendencies in the northern middle stratosphere from autumn to spring (October–April) (Fig. 8(b)). There are also significant positive correlations with O_3 tendencies in the lower stratosphere throughout this period, but for CH_4 significant correlations occur only from midwinter onwards (January) (Fig. 8(d)). In autumn significant positive correlations for CH_4 occur only above 25 km, and the region of positive correlation descends through the winter (in a similar manner to the magnitude of the variability), and by late winter significant positive correlations occur from 18 km to above 40 km.

The heat flux–tracer correlations in the southern hemisphere are similar to those in the northern hemisphere, although during southern midwinter there are weak correlations in polar regions and significant positive correlations are found around 50–70°S (in a similar location to maximum interannual variability) and the altitude above which there are positive CH_4 correlations is slightly higher (i.e. 25 km rather than 20 km). Although the latitude of maximum correlations varies with season, there are significant positive correlations between eddy heat fluxes and polar average O_3 tendencies from autumn to spring, in both the lower and middle stratosphere (Figs. 8(a) and (c)).

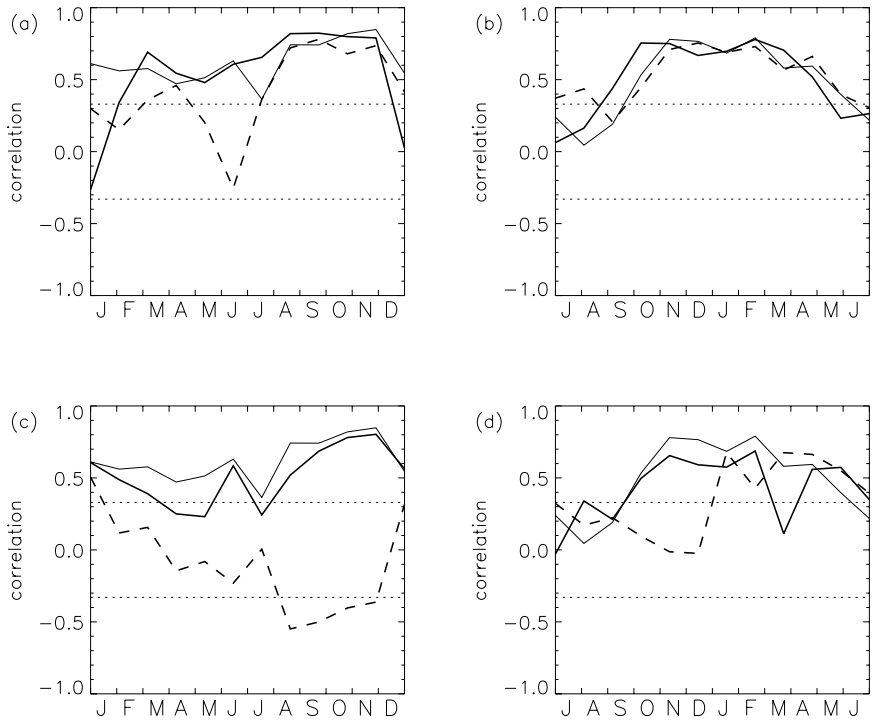

Figure 8. Seasonal variation of correlation between 100 hPa eddy heat flux, averaged between 45 and 75°, and the monthly tendency in polar average (60–90°) CH_4 (thick dashed lines) and O_3 (thick solid lines) at 29 km for (a) southern and (b) northern hemispheres. (c) and (d) are as (a) and (b) respectively, but at 22 km. Also shown is correlation between eddy heat flux and polar total column O_3 (thin solid lines). Horizontal dotted lines show correlations significant at the 95% confidence level.

The correlations with CH_4 are, however, different. Significant correlations occur only in late winter and autumn (August to November–December), with positive correlations in the middle stratosphere and negative correlations in the lower stratosphere (Figs. 8(a) and (c)).

Also shown in Fig. 8 is the correlation of polar total-column ozone and the eddy heat fluxes. There are significant positive correlations from autumn to spring in both hemispheres. The correlations between total ozone and eddy heat flux in the model are, in general, very similar to those found in recent observational studies (e.g. Fusco and Salby 1999; Randel *et al.* 2002; Weber *et al.* 2003). For example, Fig. 6 of Randel *et al.* (2002) shows significant positive correlations with polar column ozone in late winter and spring. (There are no polar ozone data in early and midwinter). Note that very similar correlations are obtained if, following Fusco and Salby (1999), an extratropical average (20–90°) is used rather than just a polar average, whereas if a midlatitude average (20–60°) is considered, the correlations are weaker and only significant for shorter periods (December to April in the northern and April to September in the southern hemisphere).

6. Concluding remarks

The analysis of methane and ozone from a 35-year simulation with no interannual variations in the external forcing or chemistry has shown that large interannual variations in stratospheric tracers can be produced by 'natural' internal dynamics within the troposphere–stratosphere system. The tracer variability is largest in the polar

stratosphere from autumn to spring, where the interannual standard deviations of CH_4 and O_3 are around 30% and 15% of the climatological mean values, respectively.

The interannual variations in the tracers and meteorology are strongly coupled, and there are global-scale variations in the temperature and tracer fields which are coherent with interannual variations in the extratropical wave driving of the stratosphere (as diagnosed by eddy heat fluxes at 100 hPa). In the stratosphere there are increased temperatures, descent and tracers in polar regions with increased wave driving, and generally the opposite response in the tropics. Statistically significant positive correlations between the wave driving and tendencies in polar (60–90°) and extratropical (20–90°) CH_4 and O_3, including total-column O_3, are found from autumn to spring in both hemispheres. These correlations in the model support recent observational studies that have shown the importance of wave driving in determining interannual variations in total ozone (e.g. Fusco and Salby 1999; Randel *et al.* 2002; Weber *et al.* 2003).

The positive tendencies in polar CH_4 associated with increased residual mean descent (and increased wave driving) are the opposite of that expected from 'unmixed descent', where increased descent would bring down lower tracer concentrations. This implies that horizontal transport processes play an important role in the interannual variations of polar tracers (see also Rosenfield and Schoeberl 2001; Strahan 2002). It is expected that increased wave driving leads to increased poleward eddy transport, as well as increased poleward and downward advection, and this poleward transport will increase the polar concentrations of both tracers. The positive correlations between wave driving and tracers hence suggests that interannual variations in polar tracers are dominated by variations in this horizontal eddy transport and not by variations in descent rates. This would then mean that interannual variations in the movement of tracer isopleths cannot be used to infer interannual variations in polar descent. However, further analysis, including possibly parcel back-trajectory calculations, as in Rosenfield and Schoeberl (2001), is required to determine the exact contributions of descent and horizontal transport in determining tracer abundances inside the polar vortex.

The quantification of the 'natural' internal tracer variability in the CH_4 and O_3 simulations in this study will provide guidance for interpreting observed tracer variability. Perhaps more importantly, this analysis will be valuable for analysis of model simulations involving interannual variations in the external forcing or chemistry, e.g. simulations with changing sea surface temperatures, chlorine loading, and/or greenhouse gases. Such model calculations are currently being performed with the GSFC 3D CTM, and comparisons with the simulation presented here will enable better quantification of the impact of variations in the forcing or chemistry.

Acknowledgement

We thank an anonymous reviewer and Susan Strahan for helpful comments. This work was partially supported by NASA grant NAG5-11283.

References

Andrews, D. G., Holton, J. R. and Leovy, C. B. 1987 *Middle Atmosphere Dynamics.* Academic Press, Oxford, UK

Austin J., Shindell D., Beagley S. R., Bruhl, C., Dameris, M., Manzini, E., Nagashima, T., Newman, P., Pawson, S., Pitari, G., Rozanov, E., Schnadt, C. and Shepherd, T. G. 2003 Uncertainties and assessments of chemistry-climate models of the stratosphere. *Atmos. Chem. Phys.*, **3,** 1–27

Boville, B. A. 1995 Middle atmosphere version of the CCM2 (MACCM2): Annual cycle and interannual variability. *J. Geophys. Res.*, **100,** 9017–9039.

Douglass, A. R. and Kawa, S. R. 1999 'GSFC 3D Chemistry and Transport Model'. Pp. 84–87 in Reports of the 1998 Models and Measurements II workshop. NASA/TM-1991-209554, Hampton, VA, USA

Douglass, A. R., Rood, R. B., Kawa, S. R. and Allen, D. J. 1997 A three-dimensional simulation of the evolution of the middle latitude winter ozone in the middle stratosphere. *J. Geophys. Res.*, **102,** 19217–19232

Fusco A. C. and Salby, M. L. 1999 Interannual variations of total ozone and their relationship to variations of planetary wave activity. *J. Atmos. Sci.*, **12,** 1619–1629

Gelman, M. E., Miller, A. J., Johnson, K. W. and Nagatani, R. M. 1986 Detection of long-term trends in global stratospheric temperature from NMC analyses derived from NOAA satellite data. *Adv. Space Res.*, **6,** 17–26

Hamilton, K. 1995 Interannual variability in the northern hemisphere winter middle atmosphere in control and perturbed experiments with the GFDL SKYHI general-circulation model. *J. Atmos. Sci.*, **52,** 44–66

Kiehl, J. T., Hack, J. J., Bonan, G. B., Boville, B. A., Williamson, D. and Rasch, P. 1998 The National Center for Atmospheric Research Community Climate Model, CCM3. *J. Climate*, **11,** 1131–1149

Langematz, U. and Pawson, S. 1997 The Berlin troposphere-stratosphere-mesosphere GCM: Climatology and forcing mechanisms. *Q. J. R. Meteorol. Soc.*, **123,** 1075–1096

Lin, S.-J. and Rood, R. B. 1996 Multidimensional Flux Form Semi-Lagrangian Transport schemes. *Mon. Weather Rev.*, **124,** 2046–2070

Lin, S.-J., Atlas, R. and Yeh, K.-S. 2004 Global weather prediction and high-end computer at NASA. *Comput. Science and Engineering*, **6,** 29–35

Newman, P. A., Nash, E. R. and Rosenfield, J. E. 2001 What controls the temperature of the Arctic stratosphere during the spring? *J. Geophys. Res.*, **106,** 19999–20010

Park, J. H., Ko, M. K. W., Jackman, C. H., Plumb, R. A., Kaye, J. A. and Sage, K. H. 1999 The atmosphere effects of stratospheric aircraft: Reports of the 1998 Models and Measurements II workshop. NASA/TM-1991-209554, Hampton, VA, USA

Pawson, S., Meyer, A. and Leder, S. 1995 Internal variability in a perpetual January integration of a troposphere–stratosphere–mesophere GCM. *Q. J. R. Meteorol. Soc.*, **121,** 369–397

Pawson, S., Kodera, K., Hamilton, K., Shepherd, T. G., Beagley, S. R., Boville, B. A., Farrara, J. D., Fairlie, T. D. A., Kitoh, A., Lahoz, W. A., Langematz, U., Manzini, E., Rind, D. H., Scaife, A. A., Shibata, K., Simon, P., Swinbank, R., Takacs, L., Wilson, R. J., Al-Saadi, J. A., Amodei, M., Chiba, M., Coy, L., de Grandpre, J., Eckman, R. S., Fiorino, M., Grose, W. L., Koide. H., Koshyk, J. N., Li, D., Lerner, J., Mahlman, J. D., McFarlane, N. A., Mechoso, C. R., Molod, A., O'Neill, A., Pierce, R. B., Randel, W. J., Rood, R. B. and Wu, F. 2000 The GCM–reality intercomparison project for SPARC (GRIPS): Scientific issues and initial results. *Bull. Am. Meteorol. Soc.*, **81,** 781–796

Prather, M. J. and Remsberg, E. E. (Eds.) 1993 The Atmospheric Effects of Stratospheric Aircraft: Report of the 1992 Models and Measurements Workshop. NASA Ref. Publ. 1292, Washington DC, USA

Randel, W. J. 1992 Global Atmospheric Circulation Statistics 1000–1 mb. NCAR Tech. Note 366, Boulder, CO, USA

1993 Global variations of zonal mean ozone during stratospheric warming events. *J. Atmos. Sci*, **50,** 3308–3321

Randel, W. J. and Wu, F. 1996 Isolation of the Ozone QBO in SAGE II data by single-value decomposition. *J. Atmos. Sci*, **53,** 2546–2559

Randel, W. J., Boville, B. A., Gille, J. C., Bailey, P. L., Massie, S. T., Kumer, J. B., Mergenthaler, J. L. and Roche, A. E. 1994 Simulation of stratospheric N_2O in the NCAR CCM2—Comparison with CLAES data and global budget analyses. *J. Atmos. Sci.*, **51,** 2834–2845

Randel, W. J., Wu, F. and Stolarski, R 2002 Changes in column ozone correlated with the stratospheric EP flux. *J. Meteorol. Soc. Jpn.*, **80,** 849–862

Randeniya, L. K., Vohralik, P. F., Plumb, I. C. and Ryan, K. R. 1997 Heterogeneous $BrONO_2$ hydrolysis: Effect on NO_2 columns and ozone at high latitudes in summer. *J. Geophys. Res.*, **102,** 23543–23557

Rind, D., Suozzo, R. and Balachandran, N. K. 1988 The GISS global climate middle atmosphere model. 2. Model variability due to interactions between planetary-waves, the mean circulation and gravity-wave drag. *J. Atmos. Sci.*, **45,** 371–386

Rosenfield, J. E. and Schoeberl, M. R. 2001 On the origin of polar vortex air. *J. Geophys. Res.*, **106,** 33485–33497

Strahan, S.E. 2002 Influence of planetary wave transport on Arctic ozone as observed by Polar Ozoner and Aerosol Measurement (POAM) III. *J. Geophys. Res.*, **107,** (20), doi: 10.1029/2002JD002189

Strahan, S. E., Nielsen, J. E. and Cerniglia, M. C. 1996 Long-lived tracer transport in the Antarctic stratosphere. *J. Geophys. Res.*, **101,** 26615–26629

Waugh, D. W., Hall, T. M., Randel, W. J., Rasch, P. J., Boville, B. A., Boering, K. A., Wofsy, S. C., Daube, B. C., Elkins, J. W., Fahey, D. W., Dutton, G. S., Volk, C. M. and Vohralik, P. F. 1997 Three-dimensional simulations of long-lived tracers using winds from MACCM2. *J. Geophys. Res.*, **102,** 21493–21513

Waugh, D. W., Randel, W. J., Pawson, S., Newman, P. A. and Nash, E. R. 1999 Persistence of the lower stratospheric polar vortices. *J. Geophys. Res.*, **104,** 27191–27201

Weber, M., Dhomse, S., Wittrock, F., Richter, A., Sinnhuber, B. M. and Burrows, J. P. 2003 Dynamical control of NH and SH winter/spring total ozone from GOME observations in 1995–2002. *Geophys. Res. Lett.*, **30,** 11, doi:10.1029/2002GL016799

Wong, S., Prather, M. J. and Rind, D. H. 1999 Seasonal and interannual variability of the budgets of N_2O and CCl_3F. *J. Geophys. Res.*, **104,** 23899–23909